Strong QCD Insights from Excited Nucleon Structure Studies with CLAS and CLAS12

D.S. Carman · K. Joo · V.I. Mokeev

Abstract Studies of the spectrum of hadrons and their structure in experiments with electromagnetic probes offer unique insight into many facets of the strong interaction in the regime of large quark-gluon running coupling, *i.e.* the regime of strong QCD. The experimental program within Hall B at Jefferson Laboratory based on data acquired with the CLAS spectrometer using electron and photon beams with energies up to 6 GeV has already considerably extended the scope of research in hadron physics in joint efforts between experiment and phenomenological data analysis. Impressive progress in relating the hadron structure observables inferred from the data to the strong QCD mechanisms underlying hadron mass generation has been achieved in the past decade. These results will be considerably extended with data from the experimental program with the new CLAS12 spectrometer that has begun data taking using electron beams with energies up to 11 GeV. With this extended kinematic reach the structure of nucleon resonances will be probed at the highest photon virtualities ever achieved in the studies of exclusive electroproduction, which will allow for the exploration of the distance scale where >98% of light hadron mass emerges from QCD in the transition of the strong interaction from the regime of quark-gluon confinement to perturbative QCD.

Keywords Excited Nucleon Structure · Nucleon Resonance Electrocouplings · Strong QCD · Emergence of Hadron Mass

1 Introduction

Significant progress has been realized in studies of excited nucleon state (N^*) structure from the data on exclusive meson electroproduction measured with the CLAS detector in Hall B at Jefferson Laboratory (JLab) [1,2,3,4]. The nucleon resonance electroexcitation amplitudes (*i.e.* the $\gamma_v p N^*$ electrocouplings) have become available for most excited nucleon states in the mass range up to 1.8 GeV for photon virtualities $Q^2 < 5$ GeV^2. These studies offer unique

D.S. Carman
Jefferson Laboratory, 12000 Jefferson Ave., Newport News, VA 23602, USA E-mail: carman@jlab.org

K. Joo
University of Connecticut, Storrs, CT 06269, USA E-mail: kyungseon.joo@uconn.edu

V.I. Mokeev
Jefferson Laboratory, 12000 Jefferson Ave., Newport News, VA 23602, USA E-mail: mokeev@jlab.org
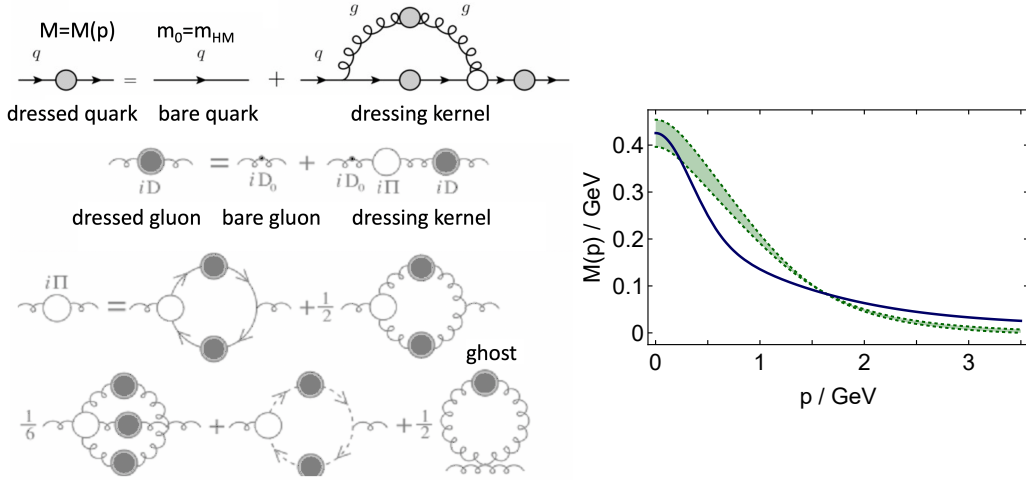
Fig. 1 (Left) The mechanisms responsible for the generation of dressed quarks and gluons from bare QCD quarks and gluons within the continuum QCD approach [8]. (Right) The momentum dependence of the dressed quark mass (green area) computed from the QCD Lagrangian compared with the fit from a phenomenological parameterization to the data on hadron spectra [9].

information on the strong QCD dynamics that govern the generation of N^* states with different quantum numbers and distinctively different structural features. The description of the structure of the ground state nucleon and the $N(1440)1/2^+$ resonance within the continuum Quantum Chromodynamics (QCD) approach with a traceable connection to QCD has demonstrated distinctive differences in their parton distribution amplitudes (PDAs) [5]. Studies of the resonant contributions to inclusive electron scattering with the resonance electroexcitation amplitudes from the CLAS data have revealed pronounced differences in their evolution with Q^2 for the invariant mass W of the final state hadrons within the first, second, and third resonance regions [6]. Therefore, the electroexcitation amplitudes of all prominent resonances in a wide range of Q^2 are of particular importance in order to explore how N^* states of different structure emerge from QCD.

Continuum QCD studies have demonstrated that the processes that are responsible for the generation of the dominant part of hadron mass have a profound impact on the Q^2-evolution of the $\gamma_v pN^*$ electrocouplings [7]. The bare QCD quarks and gauge gluons are affected by the processes imposed by the QCD Lagrangian shown in Fig. 1 (left) [8], which lead to dynamically generated dressed quarks and gluons with momentum-dependent masses. The momentum dependence of the dressed quark mass for the light u and d quarks computed within continuum QCD is shown in Fig. 1 (right) [9]. The dominant part of the dressed quark mass and, consequently, of the masses of hadrons consisting of light quarks, is generated in the regime of large QCD running coupling ($\alpha_s > 0.3$), where the dynamical quark mass increases sharply as the quark momentum decreases, producing a fully dressed light quark of mass 350-400 MeV from almost massless (few MeV) bare quarks. The dressing processes shown in Fig. 1 (left) are responsible for dynamical QCD chiral symmetry breaking (DCSB) on the hadron scale, and represent the major mechanism for the generation of hadron mass in the universe.

Gaining insight into the dressed quark mass function represents one of the most challenging tasks for experimental hadron physics. Quark-gluon confinement prevents the existence of free quarks and gluons, making direct measurements of the dressed quark mass impossible. In N^* electroexcitation, the virtual photon interaction with a dressed quark is sensitive to the quark propagator and, therefore, to the running quark mass. Consistent results on the momentum
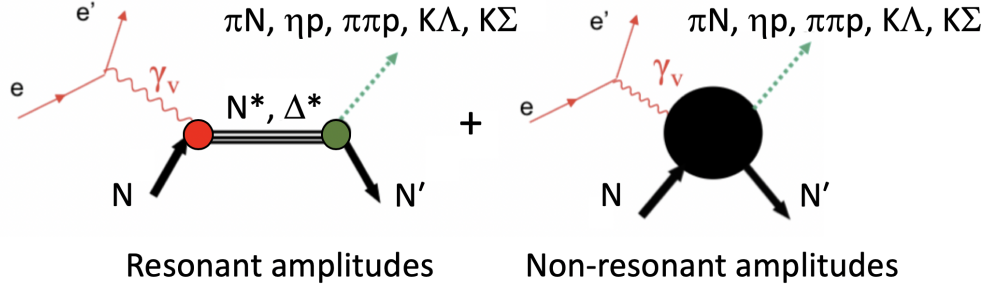
Fig. 2 Resonant and non-resonant amplitudes of exclusive meson electroproduction channels in the resonance region.

dependence of the dressed quark mass from independent studies of the pion and nucleon elastic form factors [10,11] and from the results on the Q^2-evolution of the electrocouplings of different resonances [12,13] validates the relevance of dressed quarks with a dynamically generated mass as the main structural components within the quark core of hadrons and demonstrates access to the dressed quark mass function in a nearly model-independent way [14,15]. These findings make the studies of the electrocouplings, together with the exploration of the ground state nucleon and the structure of the pion, a central emphasis in contemporary hadron physics.

2 Formalism of Exclusive Resonance Electroproduction

Nucleon resonance electroexcitation can be fully described in terms of three resonance electroexcitation amplitudes or $\gamma_v p N^*$ electrocouplings. Two of them, $A_{1/2}(Q^2)$ and $A_{3/2}(Q^2)$, describe resonance production in the process $\gamma_v p \to N^*, \Delta^*$ by transversely polarized photons of helicity $+1$ in the center-of-mass (CM) frame with the resonance spin projection directed along the γ_v momentum equal to $1/2$ and $3/2$, respectively. $S_{1/2}(Q^2)$ describes resonance electroexcitation by a longitudinal virtual photon of zero helicity with the resonance spin projection equal to $1/2$. These electrocouplings are unambiguously determined through their relation with their electromagnetic decay width to the final state with transversely Γ_γ^T and longitudinally Γ_γ^L polarized photons as:

$$\Gamma_\gamma^T(W = M_r, Q^2) = \frac{q_{\gamma,r}^2(Q^2)}{\pi} \frac{2M_N}{(2J_r + 1)M_r} \times \left(|A_{1/2}(Q^2)|^2 + |A_{3/2}(Q^2)|^2 \right),$$

$$\Gamma_\gamma^L(W = M_r, Q^2) = \frac{q_{\gamma,r}^2(Q^2)}{\pi} \frac{2M_N}{(2J_r + 1)M_r} |S_{1/2}(Q^2)|^2, \qquad (1)$$

with $q_{\gamma,r} = q_\gamma|_{W=M_r}$ the absolute value of the γ_v three momentum at the resonance point, M_r and J_r the resonance mass and spin, respectively, and M_N the nucleon mass. W is the sum of the energies of the γ_v and target proton in their CM frame. This definition of the $\gamma_v p N^*$ electrocouplings allows them to be related to the helicity amplitudes for resonance electroexcitation in any reaction model by making an identity between the resonance electromagnetic decay widths computed within the model and Eq. (1). In the same way, theory results on the resonance electroexcitation amplitudes can be converted into the electrocouplings.

Alternatively, the resonance electroexcitation can be described by three transition form factors $G_{1,2,3}(Q^2)$ or $G^*_{M,E,C}(Q^2)$. Two of them are relevant for resonances of spin-$1/2$ [2]. In the latter case, the $F^*_{1,2}(Q^2)$ Dirac and Pauli transition form factors can also be used [16], which represent Lorentz invariant functions in the most general expressions for the $N \to N^*$

transition electromagnetic currents. The description of the resonance electroexcitation in terms of the electrocouplings and the transition electromagnetic form factors is completely equivalent, since they are unambiguously related as described in Refs. [2, 16].

The resonance electrocouplings have been obtained from fits of the observables for several exclusive meson electroproduction channels within specific reaction models (see Section 3.4). The available observables include differential cross sections, as well as beam, target, and beam-target polarization asymmetries. The full amplitude of any meson electroproduction channel is given by the sum of the contributions from all resonances excited in the $\gamma_v p$ s-channel with hadronic decays to the particular final state and from the complex set of the non-resonant (background) contributions (see Fig. 2). Overall, there are six independent complex amplitudes for both single and double pseudoscalar meson and baryon final states. Data analyses within reaction models allow us to isolate the resonant contributions in the full reaction amplitudes. In turn, the resonant contributions are related to the electrocouplings that become available at the resonant point $W = M_r$ on the real energy axis. The first results on the $\Delta(1232)3/2^+$ and $N(1440)1/2^+$ electrocouplings were obtained in a global photo-/hadro-/electroproduction analysis of eight final hadron states within the advanced coupled-channel approach developed by the Argonne-Osaka group [17]. In this analysis the resonance parameters were determined from the residues at the pole positions in the complex energy plane.

3 Studies of Nucleon Resonances in Exclusive Electroproduction

Studies of nucleon resonances in different exclusive meson electroproduction channels are of particular importance for the extraction of the electrocouplings, as there are substantial differences in the non-resonant contributions in these different channels. However, the electrocouplings should be the same, since the resonance electroexcitation and hadronic decay amplitudes are independent. Therefore, consistent results on the electrocouplings from independent studies of different exclusive meson electroproduction channels is of particular importance in order to validate their reliable extraction with minimal model dependence.

Moreover, a successful description of the electroproduction data with the same, Q^2-independent, resonance masses, along with their total and partial hadronic decay widths in a wide range of Q^2, validates the resonance contributions. Several new long-awaited "missing" resonances have been discovered in analyses of exclusive meson photoproduction data [18]. In addition, the new $N'(1720)3/2^+$ resonance has recently been discovered in the combined studies of CLAS $\pi^+\pi^- p$ photo- and electroproduction data [19]. Future combined studies of meson photo-/electroproduction data will extend the available knowledge on the spectrum and structure of nucleon resonances.

Systematic studies of resonance electroexcitation became feasible only after the extensive measurements with CLAS became available for several different electroproduction channels [2, 3, 20, 21, 22]. Studies of N^* states will be extended with the new CLAS12 detector in the 12 GeV era of experiments at JLab in the range $Q^2 > 5$ GeV^2, the highest ever achieved in the study of exclusive reactions.

3.1 The CLAS and CLAS12 Detectors in Hall B

The study of the spectrum and structure of excited nucleon states with the CEBAF Large Acceptance Spectrometer (CLAS) in Hall B [23], referred to as the N^* program, represents one of the experimental physics cornerstones at JLab. In the period from 1997 to 2012 this detector was used for studies of inclusive, semi-inclusive, and exclusive reactions from a fixed

target with beams of electrons and photons at energies up to 6 GeV. The efforts of the CLAS Collaboration served to deliver on the science program, posing and sharpening questions that are central to our understanding of strong QCD.

CLAS allowed for the study of exclusive reactions in the range of Q^2 up to 5 GeV^2 and W up to 3 GeV. These data have provided has provided the dominant part of the available world information on the πN, ηp, $K\Lambda$, $K\Sigma$, and $\pi^+\pi^-p$ electroproduction channels in the resonance region ($W < 2.6$ GeV) with almost complete coverage of the final state CM phase space. The majority of the experiments were carried out with an unpolarized liquid-hydrogen target and a longitudinally polarized electron beam.

The large acceptance of this detector is of particular importance for the extraction of the electrocouplings [3, 20, 21, 22]. Around 200k data points for differential cross sections, separated structure functions, and single- and double-polarization observables have become available based on analyses of these experimental data, which are stored in the CLAS Physics Database [24]. These measurement data points continue to increase as additional analyses are completed.

In the period from 2012 to 2017 CLAS was replaced with the new large acceptance CLAS12 spectrometer [25] as part of the JLab 12 GeV upgrade project. The extended program includes a number of experiments as part of the continuing N^* program in Hall B, which will collect data over an unprecedented kinematic range for the study of nucleon excited states in the range of Q^2 from 0.05 to at least 9 GeV^2, spanning the full CM angular range of the decay final states.

Figure 3 shows model pictures of the original and the new spectrometers. The CLAS detector consisted of six equivalent azimuthal sectors around a superconducting torus magnet that spanned polar angles from $5°$ to $140°$ for beam energies up to 6 GeV. It was designed to operate with photon beams up to 1×10^7 γ/s and with electron beams at a luminosity of 1×10^{34} cm^{-2}s^{-1}. The new CLAS12 spectrometer is composed of a Forward Detector system built around a superconducting torus magnet that spans polar angles from $5°$ to $35°$ and a Central Detector built around a superconducting solenoid magnet that spans polar angles from $35°$ to $125°$. This device has been optimized for the reconstruction of exclusive reactions at beam energies up to 11 GeV. Both detectors were designed to use drift chambers for charged particle tracking, time-of-flight hodoscopes for precise timing measurements for particle identification, and a forward electromagnetic calorimeter for electron and neutral identification. In addition, CLAS12 includes a central silicon+Micromegas tracker, specialized Cherenkov systems for electron and hadron identification, and a compact forward electron tagger for quasi-real photoproduction measurements at Q^2 as low as 0.05 GeV^2. The nominal operating luminosity of CLAS12 is 1×10^{35} cm^{-2}s^{-1} in order to allow measurements at the highest possible Q^2.

3.2 Progress in Experimental Studies of πN Electroproduction

Studies of exclusive $\pi^0 p$ and $\pi^+ n$ electroproduction represent an effective tool for the exploration of the structure of excited nucleon states. Resonances in the mass range $W < 1.6$ GeV decay preferentially to πN. For these states, the studies of πN electroproduction are the driving force in the exploration of their structure. Several resonances in the mass range $W > 1.6$ GeV still have appreciable branching fractions for decays to πN. Information on the electrocouplings of these states from πN electroproduction can be compared with the results from other exclusive channels, allowing for cross checks of their systematic uncertainties.

The CLAS detector has provided the dominant part of the available world information on exclusive πN electroproduction. A total of nearly 160k data points on unpolarized differential
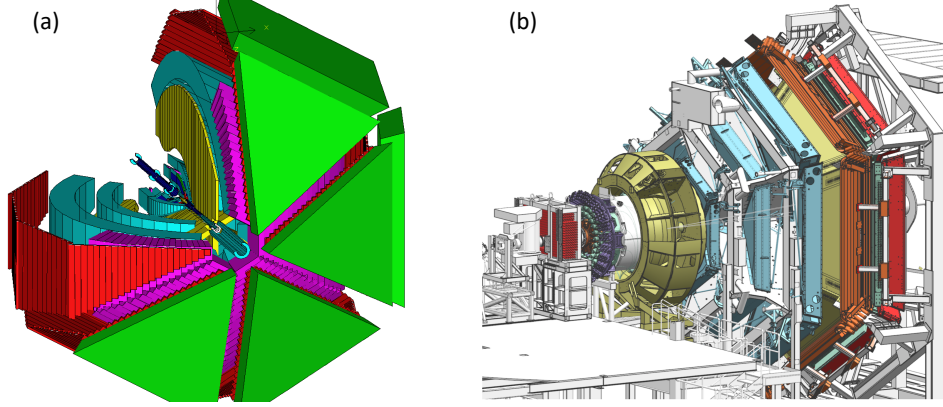
Fig. 3 (a) Model of the original CLAS spectrometer for use with electron and photon beams up to energies of 6 GeV with one of the six sectors removed to enable a view within the detector. The overall length of the detector is ∼6 m. (b) Model of the new CLAS12 spectrometer for use with electron beams up to 11 GeV. The overall length of the detector is ∼15 m.
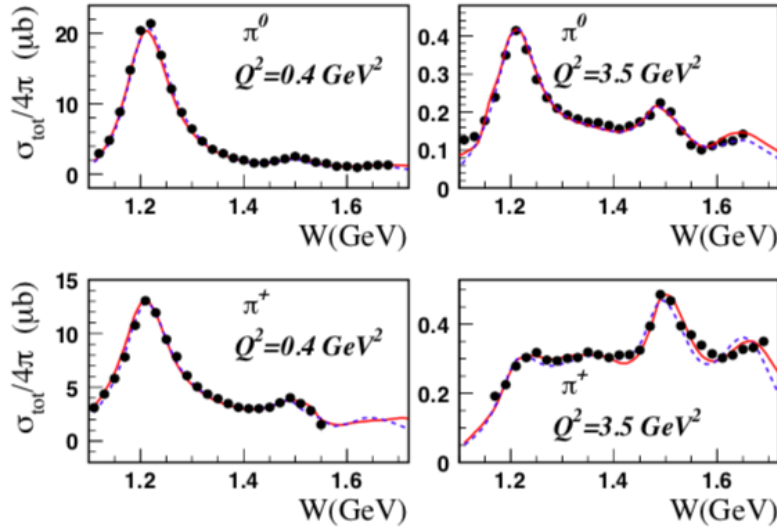

Fig. 4 $\pi^0 p$ (top) and $\pi^+ n$ (bottom) fully integrated cross sections from CLAS [28,29,30] and their description within dispersion relation (solid red line) and unitary isobar (blue dashed line) [36] models.

cross sections, longitudinally polarized beam asymmetries, and longitudinally polarized target and beam-target asymmetries have become available with almost complete coverage of the final state phase space [2,26,27,28,29,30,31,32,33,34,35]. The kinematic coverage of the πN data is presented in Table 1. Representative examples of the W dependence of the fully integrated $\pi^0 p$ and $\pi^+ n$ cross sections [28,29,30] are shown in Fig. 4.

The resonance structures in the first and second resonance regions demonstrate pronounced and different dependencies in both channels as a function of Q^2. At $Q^2 \sim 0.4$ GeV^2, the $\Delta(1232)3/2^+$ resonance represents the most pronounced structure. Instead, at $Q^2 \sim 3.5$ GeV^2, the second resonance region becomes the most pronounced structure in the $\pi^+ n$ channel, comparable with the $\Delta(1232)3/2^+$ in the $\pi^0 p$ channel. These features emphasize the sensitivity of both the $\pi^0 p$ and $\pi^+ n$ channels to the resonant contributions. Pronounced differences in the

πN Final State	W Coverage, GeV	Q^2 Coverage GeV^2	Measured Observables
$\pi^+ n$	1.1-1.38	0.16-0.36	$d\sigma/d\Omega$
	1.1-1.55	0.30-0.60	$d\sigma/d\Omega$
	1.1-1.70	1.7-4.5	$d\sigma/d\Omega$, A_b
	1.6-2.00	1.7-4.5	$d\sigma/d\Omega$
$\pi^0 p$	1.1-1.38	0.16-0.36	$d\sigma/d\Omega$
	1.1-1.68	0.40-1.80	$d\sigma/d\Omega$, A_b, A_t, A_{bt}
	1.1-1.39	3.00-6.00	$d\sigma/d\Omega$
	1.4-1.90	0.40-1.00	$d\sigma/d\Omega$

Table 1 Q^2 and W ranges covered by the CLAS πN electroproduction data and the measured observables: differential virtual photon cross sections $d\sigma/d\Omega$, and longitudinally polarized beam, target, and beam-target asymmetries, A_b, A_t, and A_{bt}, respectively.
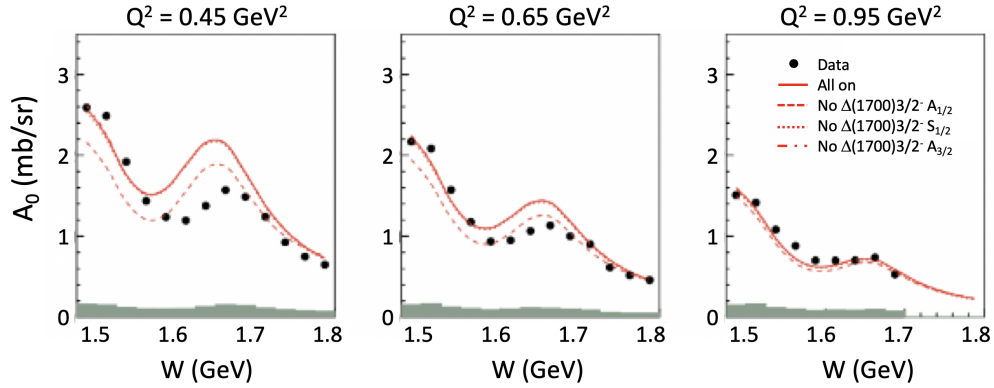
Fig. 5 A_0 Legendre moments at different Q^2 as a function of W in comparison with model calculations [36] for the electrocouplings of the resonances from the CLAS data [3,15] showing sensitivity to the $\Delta(1700)3/2^-$ by turning on/off the resonance electrocouplings. For the definition of the Legendre moments see Ref. [2].

structure of the resonances located in the first and second resonance regions are responsible for the Q^2 evolution of the πN integrated cross sections.

The isospin invariance through the Clebsch-Gordon coefficients makes the $\pi^0 p$ channel particularly sensitive to the contributions from Δ^* resonances of isospin 3/2. Precise data on differential cross sections and polarization asymmetries in the first resonance region for the $\pi^0 p$ channel has provided information on the dominant $N \rightarrow \Delta(1232)3/2^+$ magnetic transition form factor for $0.16 < Q^2 < 6.0$ GeV^2 [37]. These CLAS results provide insight into the dynamics responsible for hadron mass generation, as described in Section 4.2. Furthermore, from the studies of $\pi^0 p$ and $\pi^+ n$ electroproduction in the first resonance region, information on the R_{EM} and R_{SM} ratios of the electric quadrupole and scalar quadrupole amplitudes relative to the leading magnetic dipole amplitude, respectively, have become available [2,37]. At small Q^2, the non-zero values of R_{EM} and R_{SM} offer evidence for the departure from a spherical shape of the $\Delta(1232)3/2^+$. The behavior of these ratios at Q^2 up to 6 GeV^2 demonstrates that at this distance scale, the electroexcitation of the $\Delta(1232)3/2^+$ remains inconsistent with expectations from perturbative QCD (pQCD) [2].

Precise data on the $\pi^0 p$ and $\pi^+ n$ differential cross sections, the unpolarized, transverse-transverse, and longitudinal-transverse structure functions, as well as the results on the longitudinally polarized beam, target, and beam-target asymmetries have become available from CLAS in the second resonance region of $1.4 < W < 1.6$ GeV at $0.2 < Q^2 < 5.0$ GeV^2. Anal-

yses of these experimental data have provided precise information on the electroexcitation amplitudes of the $N(1440)1/2^+$, $N(1520)3/2^-$, and $N(1535)1/2^-$ for $Q^2 < 5$ GeV^2 for the first time [37].

Studies of πN electroproduction continue to gradually extend over W, allowing us to explore the electroexcitation amplitudes of the states in the third resonance region. Studies of $\pi^+ n$ electroproduction for $1.5 < Q^2 < 5.0$ GeV^2 [26] have provided information on the electrocouplings of the $N(1675)5/2^-$ and $N(1710)1/2^+$ for the first time and extended the results on the electrocouplings of the $N(1680)5/2^+$ to $Q^2 > 1.5$ GeV^2. These resonances decay preferentially to the πN final states and there are no close resonances of isospin 3/2 with the same spin and parity. Hence, analysis of only $\pi^+ n$ electroproduction is sufficient to extract their electrocouplings.

Recently published CLAS results on $\pi^0 p$ electroproduction for $1.4 < W < 1.9$ GeV and $0.4 < Q^2 < 1.0$ GeV^2 [27] make it possible to explore Δ^* states in the third resonance region. The substantial sensitivity of these new data to the electrocouplings of the $\Delta(1700)3/2^-$ is highlighted in Fig. 5. Here the A_0 Legendre moments from the $\pi^0 p$ cross sections are compared with model expectations [36] when the electrocouplings of this Δ^* state available from the $\pi^+ \pi^- p$ data [3,15] are turned on/off.

The CLAS $\pi^+ n$ data should be extended within the range $1.4 < W < 1.9$ GeV and $0.4 < Q^2 < 1.0$ GeV^2 covered by the $\pi^0 p$ data [27]. Also, data from the $\pi^0 p$ channel should be made available for $1.4 < W < 2.0$ GeV and $1.5 < Q^2 < 5.0$ GeV^2 covered by the existing $\pi^+ n$ data [2,26]. The combined analysis of the $\pi^+ n$ and $\pi^0 p$ data in the same range of W and Q^2 within the available models [36] represents an important part of the efforts aimed at obtaining the electrocouplings of the states in the third resonance region with isospin $I = 1/2$ and 3/2. These data also provide important input for the development of coupled-channel analyses.

3.3 $\pi^+ \pi^- p$ and KY Exclusive Electroproduction in the Resonance Region

The $\gamma_v p \rightarrow \pi^+ \pi^- p$ electroproduction channel is sensitive to the most excited states observed so far in the N^* spectrum. N^* states in the mass range <1.6 GeV decay mostly to πN final states [38], making the πN electroproduction channels the primary source of information on their electrocouplings. However, these low-lying resonances, except for the $N(1535)1/2^-$, also have significant branching fractions (above 30%) for decays into the $\pi\pi N$ final states, which also makes it possible to evaluate their electrocouplings through $\pi^+ \pi^- p$ photo-/electroproduction in this channel. Consistent results on the electrocouplings of nucleon resonances determined from independent studies of the πN and $\pi^+ \pi^- p$ channels allow for cross checks of systematic uncertainties, in particular those associated with the reaction models.

Studies of $\pi^+ \pi^- p$ electroproduction are of particular importance in order to gain insight into the electrocouplings of N^* states in the third resonance region. Here, the $\Delta(1620)1/2^-$, $\Delta(1700)3/2^-$, and $N(1720)3/2^+$ have branching fractions for decays of >50%. For this final state, the branching fractions for many resonances in the third resonance region have been established with large uncertainties [38]. However, almost all resonances in the mass range from 1.6 GeV to 1.75 GeV, except for the $N(1675)5/2^-$ and $N(1710)1/2^+$, have a measurable impact on the $\pi^+ \pi^- p$ observables, making studies of this exclusive channel an important tool for insight into the electroexcitation amplitudes of most states in the third resonance region. Furthermore, a successful description of $\pi^+ \pi^- p$ electroproduction data with Q^2-independent resonance hadronic decay widths allows us to improve the knowledge on hadronic decays of these states [15,19].

According to the quark model results on the hadronic decays of N^* states [39,40], studies of $\pi^+ \pi^- p$ photo-/electroproduction offer promising opportunities in the search for the miss-

| Q^2 Coverage, GeV^2	W Coverage, GeV	W/Q^2 Bin Size GeV/GeV^2	Data Status
0.	1.6-2.0	0.25/N.A.	Completed [41]
0.2-0.6	1.30-1.57	0.025/0.050	Completed [42]
0.5-1.5	1.40-2.10	0.025/0.3-0.4	Completed [43]
0.4-1.0	1.30-1.85	0.025/0.050	Completed [44]
2.0-5.0	1.40-2.00	0.025/0.5	Completed [45]
2.0-5.0	1.40-2.00	0.025/0.5	In progress [46]

Table 2 Kinematic area in Q^2 and W covered by the CLAS measurements of the $\pi^+\pi^-p$ photo-/electroproduction cross sections and the associated data references.

ing resonances. The existence of these states is predicted based on the approximate SU(6) symmetry of the strong interaction relevant in the regime of strong QCD. Searches for these states for a long time have been a challenging task. Recently, a new $N'(1720)3/2^+$ resonance was observed in the combined studies of $\pi^+\pi^-p$ photo- and electroproduction data [19], in addition to several new missing resonances discovered in a global multi-channel analysis of meson photo- and hadroproduction [18]. For the first time the results on the electrocouplings of the missing $N'(1720)3/2^+$ resonance have become available, offering insight into its internal structure.

The CLAS detector has provided the only available world data on the nine independent, unpolarized 1-fold differential $\pi^+\pi^-p$ photo- and electroproduction cross sections in the broad kinematic range of W and Q^2 listed in Table 2. Representative examples of these differential cross sections in a particular bin of W and Q^2 are shown in Fig. 6. They consist of invariant mass distributions for the three pairs of final state hadrons, three CM angular distributions for the final state hadrons, and three CM distributions for the angles between the reaction plane for one of the final state hadrons with the target proton and a second plane defined by the three momenta of the other two final state hadrons. The kinematics of the $\pi^+\pi^-p$ state is fully determined by 5 independent variables. The nine 1-fold differential cross sections represent the integrals from the common 5-fold differential cross sections over different sets of 4 variables. In recent studies [46], nine transverse-transverse and transverse-longitudinal contributions into the $\pi^+\pi^-p$ electroproduction cross sections have become available along with the nine unpolarized cross sections.

The CLAS data on $\pi^+\pi^-p$ electroproduction have provided the first results on the electrocouplings of the $N(1440)1/2^+$ and $N(1520)3/2^-$ at $Q^2 < 0.55$ GeV^2 [42]. Analysis of other $\pi^+\pi^-p$ data [43] have extended the information on these electrocouplings in the Q^2 range up to 1.5 GeV^2 and provided results on the electrocouplings of the $\Delta(1620)1/2^-$ [15], as well as preliminary results on the electrocouplings of the $N(1680)5/2^+$, $\Delta(1700)3/2^-$, and $N(1720)3/2^+$ [3,20,43]. Analysis of the highest precision $\pi^+\pi^-p$ data [44], collected in Q^2 bins as small as 0.05 GeV^2 (see Table 2) will further improve our knowledge of N^* electroexcitations in the third resonance region. Analysis of these data [45,46] will provide information on the electrocouplings of all resonances in the mass range up to 2 GeV that are prominent for $2 < Q^2 < 5$ GeV^2 and will shed light on the manifestations of new baryon states, including those seen through a global multi-channel analysis of exclusive photoproduction [18].

The recent advancements in understanding the spectrum and structure of the nucleon excited states have mainly been provided by advanced analyses of the exclusive πN, $\pi\eta$, and $\pi^+\pi^-p$ reaction channels. However, with the publication of the high quality $K^+\Lambda$ and $K^+\Sigma^0$ photoproduction data from CLAS [47,48,49,50], the potential and importance of the hyperon channels has been demonstrated. In fact, the spectrum of N^* states listed in the recent edition of the Particle Data Group (PDG) [38] has been radically altered by the K^+Y photoproduction
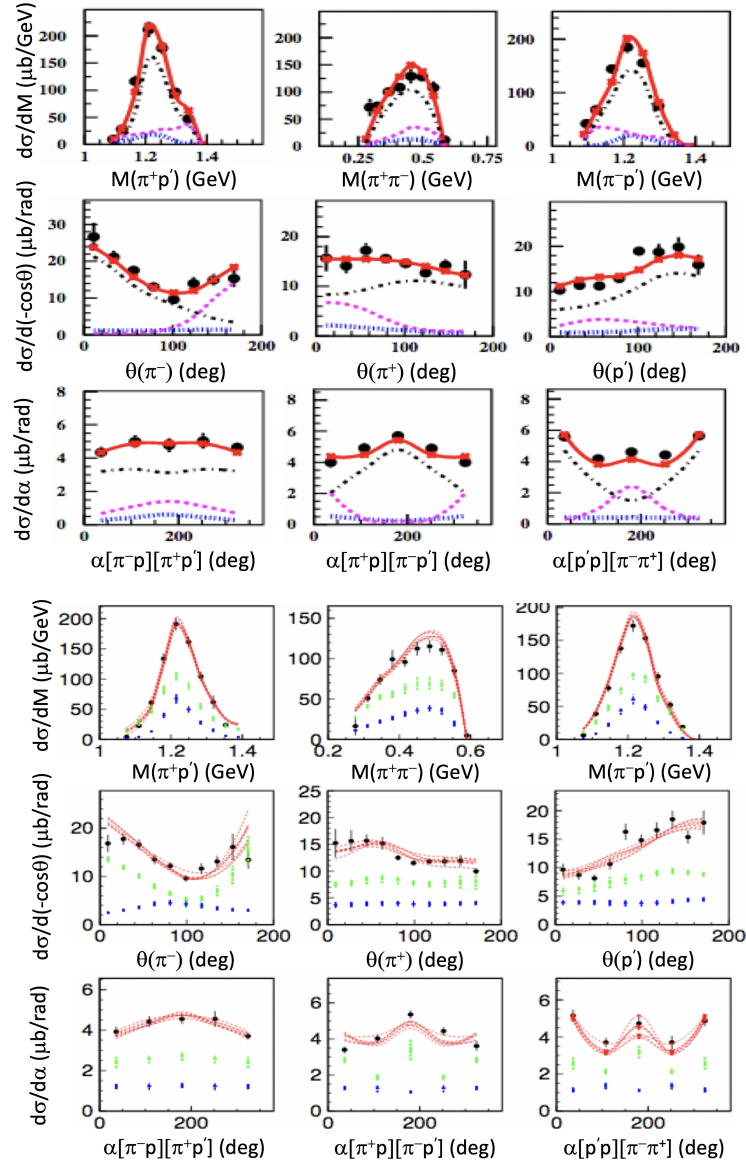
Fig. 6 Nine 1-fold differential $\pi^+\pi^-p$ electroproduction cross sections measured with CLAS at W=1.51 GeV and Q^2= 0.65 GeV^2 [43]. (Top) Data description [15] within the JM model outlined in Section 3.4.2 (red solid lines) and the contributing meson-baryon channels with amplitudes established from the data: $\pi^-\Delta^{++}$ (black dot-dashed), $\pi^+\Delta^0$ (blue dashed), 2π direct production (magenta dashed). (Bottom) Fit of the data within the JM model. Selected cross sections computed in the data fit are shown by the red dashed curves. The resonant/non-resonant contributions determined in the data fit are shown by the blue/green bars.

data, including both differential cross sections and polarization observables. Table 3 shows a comparison of the current PDG listings for a dozen N^* and Δ^* states compared to just a decade ago. For most of these states the K^+Y data were of critical importance in the update. The $K^+\Lambda$ and $K^+\Sigma^0$ channels are important to consider separately. Although the two ground-state hyperons have the same valence quark content (uds), they differ in isospin ($I=0$ for Λ and $I=1$ for Σ^0), so that N^* states of $I = 1/2$ can decay to $K^+\Lambda$, but Δ^* states cannot. Because both N^* and Δ^* resonances can couple to the $K^+\Sigma^0$ final state, the hyperon final state selection constitutes an isospin filter.

State $N(mass)J^P$	PDG pre-2010	PDG 2018	πN	$K\Lambda$	$K\Sigma$	γN
$N(1710)1/2^+$	***	****	****	**	*	****
$N(1875)3/2^-$		***	**	*	*	**
$N(1880)1/2^+$		***	*	**	**	**
$N(1895)1/2^-$		****	*	**	**	****
$N(1900)3/2^+$	**	****	**	**	**	****
$N(2000)5/2^+$	*	**	*			**
$N(2060)5/2^-$		***	**	*	*	***
$N(2100)1/2^+$	*	***	***	*		**
$N(2120)3/2^-$		***	**	**	*	***
$\Delta(1600)3/2^+$	***	****	***			****
$\Delta(1900)1/2^-$	**	***	***		**	***
$\Delta(1940)3/2^-$	*	**	**			*.
$\Delta(2200)7/2^-$	*	***	**		**	***

Table 3 Evolution of our understanding of the excited N^* and Δ^* spectrum over the past decade and the available evidence from different initial/final states based on the PDG "*" ratings in the pre-2010 and 2018 listings. Note also that our knowledge of more than a dozen additional states in the most recent PDG listings (not shown here), while remaining unchanged in their overall * rating, have now been improved by quantifying their coupling to additional initial/final states compared to the pre-2010 listings. The KY channels have been a vital inclusion in this expansion of our understanding.

Beyond the available KY photoproduction data, the KY electroproduction data are by far the most extensive and precise measurements within the nucleon resonance region $1.6 < W < 2.6$ GeV [51,52]. They are of great value for independent extractions of the resonance electrocouplings available from the πN and $\pi^+\pi^-p$ electroproduction data at $W > 1.6$ GeV. Measurements have been provided for the differential cross sections and separated structure functions σ_T, σ_L, $\sigma_U = \sigma_T + \epsilon\sigma_L$, σ_{LT}, σ_{TT}, and $\sigma_{LT'}$ for $K^+\Lambda$ and $K^+\Sigma^0$ [53,54,55, 56], recoil polarization for $K^+\Lambda$ [57], and beam-recoil transferred polarization for $K^+\Lambda$ and $K^+\Sigma^0$ [58,59]. These data span Q^2 from 0.5 to 4.5 GeV^2, W from 1.6 to 3 GeV, and the full CM angular range of the K^+. KY exclusive production is sensitive to coupling to higher-lying N^* states for $W > 1.6$ GeV. It is precisely in this mass range where our knowledge of the N^* spectrum is the most limited. These data have comparable uncertainties as for the available CLAS $\pi^+\pi^-p$ electroproduction data and can also be used to confirm the signals of new baryon states observed in photoproduction in a complementary fashion by checking whether within each bin of Q^2, the determined states have the same masses and decay widths. Reliable information on the electrocouplings from the KY channels is not yet available due to the lack of a suitable reaction model. Further development of reaction models [60,61], as well as other approaches that will make it possible to employ them for the extraction of the resonance electrocouplings from the KY electroproduction data is critically needed in order to make progress with these important channels.

3.4 Approaches for Evaluation of Resonance Electrocouplings from Data

Most of the results on the $\gamma_v pN^*$ electrocouplings have become available from independent analyses of the major exclusive meson electroproduction channels $\pi^+ n$, $\pi^0 p$, and $\pi^+\pi^- p$ [2, 3, 20, 62, 63, 64]. The electrocouplings of the $N(1535)1/2^-$ were also obtained from the data on ηp electroproduction [65]. The first results on the electrocouplings of the $\Delta(1232)3/2^+$ and $N(1440)1/2^+$ at their pole positions were determined in a global 8-channel analysis of exclusive meson electro- and hadroproduction data developed by the Argonne-Osaka group [17]. These breakthrough results should be extended in the future for other excited nucleon states. In this Section we consider approaches developed by the CLAS Collaboration for the extraction of the electrocouplings from the data on exclusive πN and $\pi^+\pi^- p$ electroproduction.

### 3.4.1 Electrocoupling Extraction from CLAS πN Electroproduction Data

The extraction of the electrocouplings from the CLAS $\pi^0 p$ and $\pi^+ n$ electroproduction data was carried out within two different approaches that used a) a dispersion relation technique (DR) and b) the Unitary Isobar Model (UIM) [36, 37].

In the DR approach, exclusive πN electroproduction has been described by six independent Lorentz invariant functions in the most general expression for the transition $N \to \pi N$ electromagnetic current. These functions, the so-called Ball amplitudes, are defined in Ref. [2]. Each Ball amplitude $B_i(s,t)$ (i=1,2,3,6,8) and $B_5'(s,t)$ in both the $\pi^0 p$ and $\pi^+ n$ channels represents a complex function of the Mandelstam variables s and t. At fixed values of t and Q^2 the real part of the amplitudes $Re[B_i(s,t)]$ can be expressed through their imaginary parts $Im[B_i(s,t)]$ by employing dispersion relations [2, 36, 37]. For the B_3 amplitudes, what is known as the subtraction procedure was employed in the dispersion relations in order to provide a zero value for the dispersive integrand at absolute values of s in the complex energy plane that tend to infinity. This procedure invokes a phenomenological subtraction function $f_{sub}(t, Q^2)$ fit to the data. For the description of the πN reaction from both protons and neutrons, and accounting for isospin, we have 15 unsubtracted and 1 subtracted dispersion relations, which are based just on the most general principles of analyticity and crossing symmetry for the reaction amplitudes. The amplitude singularities and residues that enter into the dispersion relations were obtained assuming pion exchange in the t-channel and nucleon exchange in the s-channel as shown in Fig. 7. Eventually, pion exchange in the t-channel was reggeized. It was found that for $W > 1.3$ GeV, the $Im[B_i(s,t)]$ in πN electroproduction were well described by the resonant contributions only. This makes it possible to evaluate all Ball amplitudes from the resonance parameters by employing fixed-t dispersion relations independently at different Q^2. For $W < 1.3$ GeV the non-resonant contributions, which become sizable in the Ball amplitudes, were evaluated by using the Watson theorem from the measured phases of the πN elastic scattering amplitudes.

Within the UIM the full πN electroproduction amplitudes are described by the resonant contributions and the non-resonant Born terms shown in Fig. 7 [2, 36]. The s- and u-channels incorporate nucleon exchange. The t-channel includes π, ρ, and ω exchanges. The reggeized π, ρ, ω, b_1, and a_2 contributions are also employed in the description of the t-channel amplitudes. The full non-resonant amplitudes represent the sum of the Born pole terms and the reggeized t-channel contributions with the relative weights fit to the data and detailed in Ref. [2]. The non-resonant contributions are unitarized within the K-matrix approach [36] assuming πN rescattering for the final state interaction. The resonant contributions are described within the Breit-Wigner ansatz with W-dependent N^* electromagnetic, πN, and total decay widths. The electrocouplings were fit to the measured observables within the UIM approach. The uncertainties of the electrocouplings account both for the statistical/systematic data uncer-
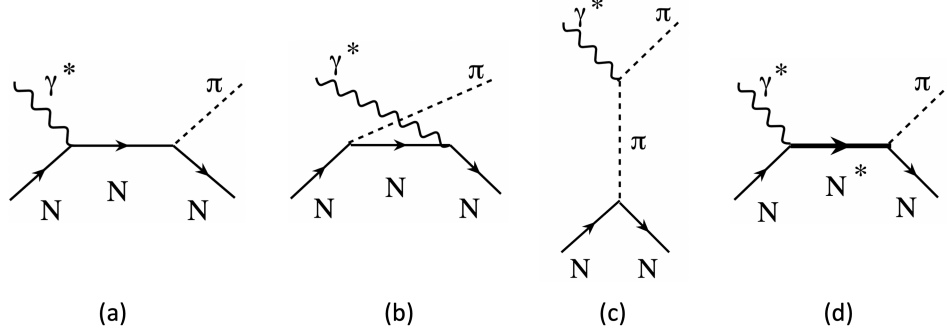
Fig. 7 Born terms (a, b, c) and the resonant contribution (d) for the description of $\pi^0 p$ and $\pi^+ n$ electroproduction in Refs. [2, 36, 37].
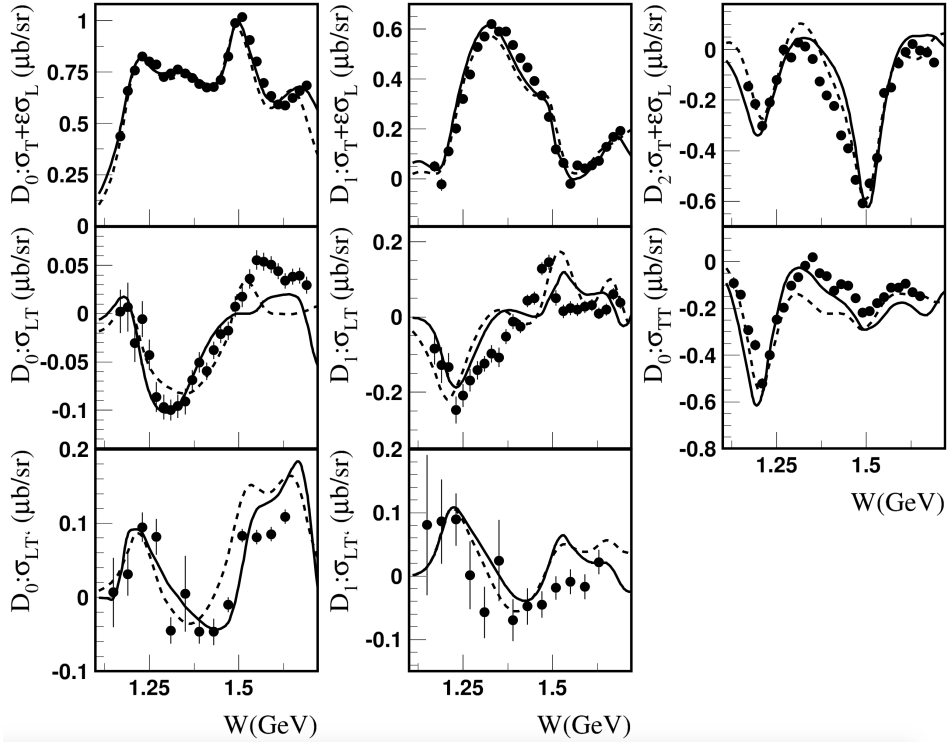
Fig. 8 Legendre moments of the $\pi^+ n$ structure functions at $Q^2 = 2.05$ GeV^2. The experimental results from Ref. [30] are compared with the computations of the DR (solid lines) and UIM (dashed lines) approaches in Ref. [36].

tainties, as well as the accuracy of the knowledge on the resonance hadronic decays and the electromagnetic and hadronic vertices in the non-resonant amplitudes.

Both the DR and UIM approaches provide a good description of all πN electroproduction data measured with CLAS at $W < 1.8$ GeV and $0.16 < Q^2 < 5.0$ GeV^2. Representative examples are shown in Fig. 4 and Fig. 8 for the description of the fully integrated πN cross sections and for the Legendre moments of the exclusive πN structure functions, respectively.

Differences in the electrocouplings determined within the DR and UIM approaches provide an estimate for the systematic uncertainties of these quantities determined from the different reaction models.

3.4.2 Electrocoupling Extraction from CLAS $\pi^+\pi^-p$ Electroproduction Data

The analysis of the exclusive $\pi^+\pi^-p$ photo- and electroproduction data from CLAS was carried out within the data-driven meson-baryon JLab-Moscow (JM) model [66,67]. The wealth of these data on the nine 1-fold differential $\pi^+\pi^-p$ cross sections allows us to establish all relevant mechanisms that contribute to this exclusive channel from their manifestations in the observables, such as peaks in the invariant mass distributions and pronounced dependencies in the CM angular distributions (see Fig. 6 (top)). The mechanisms with less pronounced kinematic dependencies can be pinned down from the correlations between their contributions in the different differential cross sections. Within this strategy, the phenomenological JM model has been developed with a primary objective to determine the resonance $\gamma_{r,v}pN^*$ photo-/electrocouplings and the resonance decay widths to the $\pi\Delta$ and ρp final states.

Within the JM model, the full 3-body $\pi^+\pi^-p$ electroproduction amplitude incorporates the contributions from five meson-baryon channels: $\pi^-\Delta^{++}$, ρp, $\pi^+\Delta^0$, $\pi^+N^0(1520)3/2^-$, and $\pi^+N^0(1685)5/2^+$, with subsequent decays of the unstable intermediate hadrons. It also contains direct 2π photo-/electroproduction processes where the final $\pi^+\pi^-p$ state is created without the generation of unstable intermediate hadrons. Here the nucleon resonances contribute to the $\pi^-\Delta^{++}$, $\pi^+\Delta^0$, and ρp meson-baryon channels. Modeling of the non-resonant contributions is described in Refs. [66,67,68,69]. The model includes the contributions from all four-star PDG resonances with observed decays to the $\pi\pi N$ final states, the $N(1700)3/2^-$, and the new $N'(1720)3/2^+$ [19]. The resonant amplitudes are described within the unitarized Breit-Wigner ansatz [67] to make them consistent with the restrictions imposed by a general unitarity condition. The JM model offers a good description of the $\pi^+\pi^-p$ differential cross sections in the entire kinematic area covered by the data are shown in Table 2. A representative example of the data description is shown in Fig. 6, along with the differential cross sections for the different contributing mechanisms inferred from the data.

The resonance parameters were determined from a fit to the nine 1-fold differential cross sections under simultaneous variation of the photo-/electrocouplings, masses, total and partial hadronic decay widths to the $\pi\Delta$ and ρp final states, and the non-resonant parameters of the JM model. The uncertainties of the resonant contributions are comparable with the uncertainties of the measured cross sections, which provides evidence for the reliable evaluation of these contributions and their photo-/electrocouplings.

3.5 CLAS Electrocouplings from Exclusive Meson Electroproduction Data

The electrocouplings of N^* states with masses below 1.8 GeV have been determined from analyses of CLAS πN, ηN, and $\pi\pi N$ data for Q^2 up to 5 GeV^2. See Table 4 for a summary of the results. A parameterization of these electrocouplings for this kinematic range is given in Ref. [6].

The most detailed information on the electrocouplings is currently available for the N^* states in the mass range $W < 1.6$ GeV from studies of πN, ηN, and $\pi^+\pi^-p$ photo-/electroproduction for Q^2 up to 7.7 GeV^2 for the $\Delta(1232)3/2^+$ and for Q^2 up to 7 GeV^2 for the $N(1535)1/2^-$ [37, 65,70,71], and for $Q^2 < 5$ GeV^2 for other resonances [37]. The electrocouplings for the $N(1440)1/2^+$ and $N(1520)3/2^-$ available from independent studies of πN and $\pi^+\pi^-p$ electroproduction are shown in Fig. 9. These precise results for πN and $\pi^+\pi^-p$ for Q^2 up to

| Exclusive Electroproduction Channel	Nucleon Resonance	Q^2 Range for $\gamma_v p N^*$ Electrocouplings
$\pi^0 p$, $\pi^+ n$	$\Delta(1232)3/2^+$	0.16-6.0
	$N(1440)1/2^+$, $N(1520)3/2^-$, $N(1535)1/2^-$	0.30-4.5
$\pi^+ n$	$N(1675)5/2^-$, $N(1680)5/2^+$ $N(1700)1/2^+$	1.6-4.5
ηp	$N(1535)1/2^-$	0.20-2.9
$\pi^+ \pi^- p$	$N(1440)1/2^+$, $N(1520)3/2^-$,	0.25-5.0
	$N(1520)3/2^-$, $\Delta(1620)1/2^-$, $N(1650)1/2^-$, $N(1680)5/2^+$, $\Delta(1700)3/2^-$, $N(1720)3/2^+$, $N'(1720)3/2^+$	0.50-1.5

Table 4 N^* states for which the $\gamma_v p N^*$ electrocouplings are available from the CLAS exclusive meson electroproduction data showing the final state channel and the Q^2 range of the data.

5 GeV^2 agree to within the data uncertainties for most data points. Consistent results on the electrocouplings from these two channels, which have entirely different non-resonant contributions, validates their extraction. Furthermore, this success demonstrates the capabilities of the reaction models discussed in Section 3.4 for the reliable extraction of the resonance parameters from independent studies of these two channels.

Studies of $\pi^+ n$ and $\pi^+ \pi^- p$ exclusive electroproduction have provided complementary information on the electrocouplings of the N^* states in the third resonance region. The electrocouplings of the $N(1675)5/2^-$, $N(1680)5/2^+$, and $N(1700)1/2^+$ were determined for $1.6 < Q^2 < 4.5$ GeV^2 from $\pi^+ n$ electroproduction [26]. For the first time, the electroexcitation amplitudes of the $\Delta(1620)1/2^-$ [15], $N(1720)3/2^+$, $N'(1720)3/2^+$, and $\Delta(1700)3/2^-$ [19], which decay preferentially to the $\pi\pi N$ final state, have become available. Recently, new results on the exclusive structure functions for $\pi^0 p$ electroproduction have also been obtained [27], together with the precise data from CLAS on the nine 1-fold differential $\pi^+ \pi^- p$ cross sections [44]. These observables have been obtained from the same data set measured for $1.4 < W < 1.85$ GeV and $0.4 < Q^2 < 1.0$ GeV^2 for both the πN and $\pi^+ \pi^- p$ channels. These data considerably extend the opportunities for the exploration of the electroexcitation amplitudes of the states in the third resonance region.

A successful description of all of the CLAS nine 1-fold $\pi^+ \pi^- p$ differential cross sections available in the range $1.4 < W < 2.0$ GeV and $2.0 < Q^2 < 5.0$ GeV^2 [45,46] has been achieved within the updated version of the JM model [20,21]. This success offers good prospects for the extraction of the electrocouplings for most excited nucleon states over this entire kinematic range.

These studies have made it apparent that consistency of the results from independent analyses of multiple exclusive channels is necessary to have confidence in the results. For the hadronic couplings, many high-lying N^* states preferentially decay through the $\pi\pi N$ channel. For these states data from the KY channels already measured with CLAS will be crucial to provide an independent analysis to compare the extracted electrocouplings for the high-lying N^* states against those determined from the πN and $\pi\pi N$ channels for Q^2 up to 5 GeV^2.
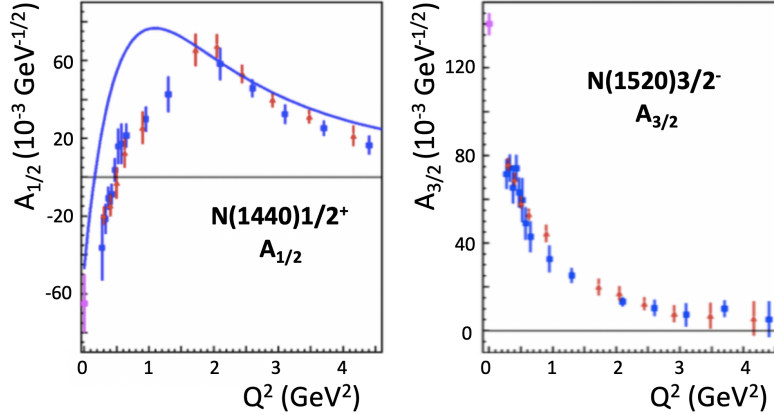
Fig. 9 Electrocouplings of the $N(1440)1/2^+$ and $N(1520)3/2^-$ from independent analyses of the πN (red triangles) [37] and $\pi^+\pi^- p$ electroproduction channels (blue squares) [15, 20, 67]. The $A_{1/2}(Q^2)$ electrocoupling for the $N(1440)1/2^+$ computed within the continuum QCD approach [14, 72] is shown by the solid line. The region at $Q^2 > 1.5$ GeV^2 is the regime of quark core dominance.

4 Insight into Strong QCD from Nucleon Resonance Electrocouplings

4.1 Charting Active Degrees of Freedom in N^* Structure

Detailed studies of the structure of most prominent nucleon resonances from the experimental results on their electroexcitation amplitudes have played a central role in the development of our understanding of how the strong interaction generates these states from quarks and gluons [1, 2, 73, 74]. The concept of the structure of N^* states as bound systems of three constituent quarks that has emerged through such studies led to the development of the constituent quark model for nucleon resonances [75, 76] (CQM) in the 1980s. As a result of intense experimental and theoretical effort over the past 30 years, it is now apparent that the structure of the nucleon and its spectrum of excited states is much more complex than what can be described in terms of the models based on constituent quarks alone [1, 2, 16, 77, 78, 79].

As shown in Fig. 10, the approaches that take into account the contributions from dressed (constituent) quarks only are able to describe the experimental results on the electrocouplings for $Q^2 > 2$ GeV^2 (except for the $N(1675)5/2^-$), but they fail in reproducing the results for $Q^2 < 1$ GeV^2. The additional contributions to the structure of the states that are the most relevant at low Q^2 come from the meson-baryon cloud generated in the processes depicted in Fig. 10 (bottom right). For the $\Delta(1232)3/2^+$, the meson-baryon cloud contributions were inferred from the coupled-channel analyses of exclusive meson photo-, electro-, and hadroproduction data [80, 81]. Only after accounting for the contributions from both the core of three dressed quarks and the meson-baryon cloud were the results reproduced for the $N \to \Delta(1232)3/2^+$ transition magnetic form factor in the entire Q^2-range covered by the measurements (see Fig. 10 (top left)). The continuum QCD Dyson Schwinger (DSE) approach offers a good description of the quark core contribution to the $N(1440)1/2^+$ structure for $Q^2 > 2$ GeV^2 starting from the QCD Lagrangian [12, 13, 14]. This success allowed for the evaluation of the meson-baryon cloud contributions as the difference between the experimental results on the $N(1440)1/2^+$ electroexcitation amplitude and the expectations from DSE on the quark core contributions. As shown in Fig. 10 (top right), the quark core contributions to the $N(1440)1/2^+$ $A_{1/2}$ electrocoupling evaluated within the light front quark model [83], which
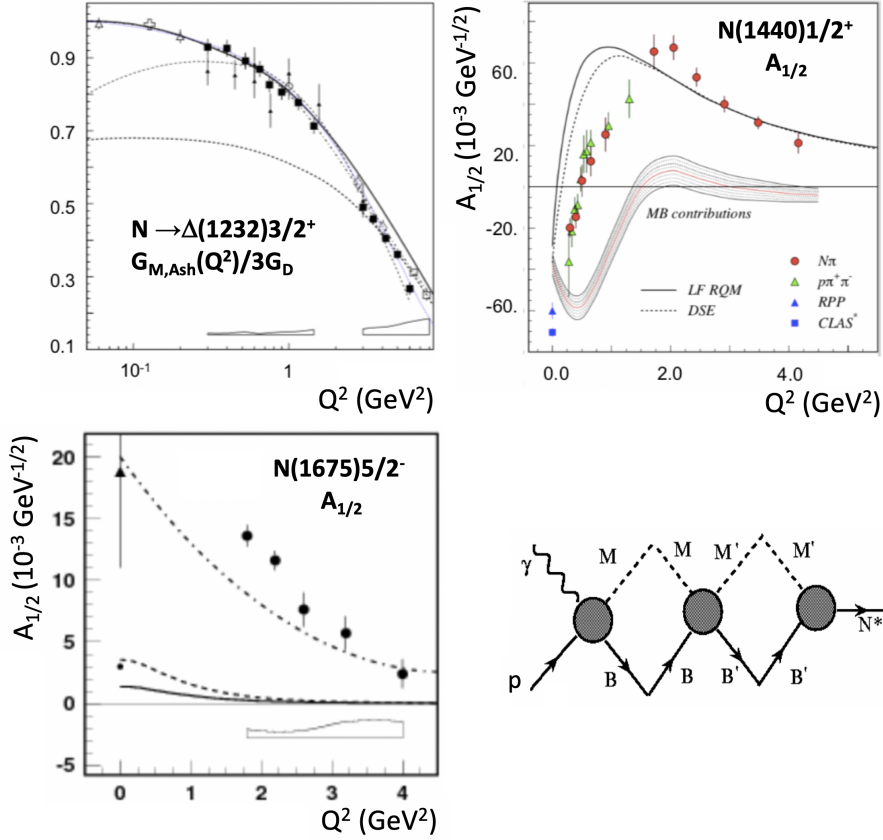
Fig. 10 Meson-baryon cloud and quark core in the structure of different resonances. (Top left) Data from the review of Ref. [2] on the $N \to \Delta$ magnetic transition form factor in the Ash convention $G^*_{M,Ash}$ normalized to the dipole fit of the ground state nucleon form factor $3G_D$ in comparison with model predictions [80, 81] that account for the contributions from the combined quark core and meson-baryon cloud (solid line) and from the quark core only (thick dotted line). The evaluations from the large N_C limit of QCD that incorporate a substantial part of the meson-baryon cloud [82] are shown by the dot-dashed and thin dotted lines. (Top right) CLAS results on the $A_{1/2}$ electrocouplings of the $N(1440)1/2^+$ [15, 37, 67] compared to the quark core contributions computed within the light-front relativistic quark model [83] (solid line) and within continuum QCD DSE [14] (dotted line). The meson-baryon cloud estimated as the difference between the experimental results and the light front quark model results for the quark core [83] is shown by the shadowed area. (Bottom left) $A_{1/2}$ electrocouplings of the $N(1675)5/2^-$ from CLAS data [84] compared to the contributions from the quark core evaluated within the hypercentral [85] (solid line) and Bethe-Salpeter [86] (dotted line) quark models. The meson-baryon cloud estimated within the Argonne-Osaka coupled-channel approach [87] is shown by the dot-dashed line. (Bottom right) The amplitudes that generate the meson-baryon dressing.

employs the phenomenological quark mass function, are in good agreement with the DSE results [14] at $Q^2 > 2.0$ GeV^2. The meson-baryon cloud contributions to the $N(1440)1/2^+$ $A_{1/2}$ electrocoupling estimated as the difference between the experimental data and quark core contribution from the light front quark model [83] is shown by shadowed area in Fig. 10 (top right). The meson-baryon cloud becomes the biggest contribution for $Q^2 < 1$ GeV^2, but almost vanishes for $Q^2 > 2$ GeV^2. The important role of the meson-baryon cloud in the structure of $N(1440)1/2^+$ was also demonstrated in recent lattice QCD studies that pave the way for the exploration of the emergence of the meson-baryon cloud [88]. These studies have demonstrated that the structure of the $N(1440)1/2^+$ is defined by a core of three dressed quarks in their
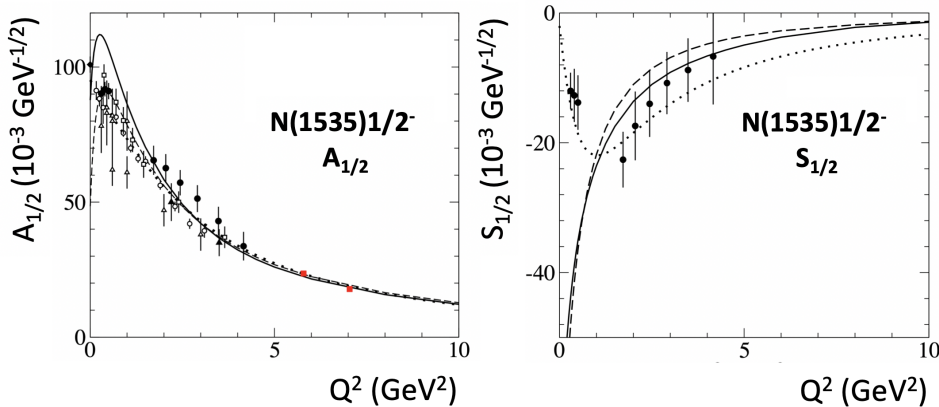
Fig. 11 Improvements in the description of the results on the $\gamma_v p N^*$ electrocouplings [37,71] achieved after accounting for the contributions of the meson-baryon cloud and the quark core. A description of the $N(1535)1/2^-$ is shown for the relativistic quark model [16] accounting for the contributions from $K\Lambda$ loops and the quark core (solid lines) and the quark core only (dashed line). The AdS/CFT results [79] are shown by the dotted lines.

first radial excitation, surrounded by an external meson-baryon cloud, and they have resolved the more than fifty year old puzzle on the structure of this state [1].

For other resonances studied with CLAS, the contributions from the meson-baryon cloud were taken into account within the model approaches [16,74,78,79,83]. Accounting for both dressed quarks and the meson-baryon cloud contributions offers an improved description of the electrocoupling results, in particular for $Q^2 < 1$ GeV^2 (see Fig. 11). The anti-de Sitter/conformal field theory (AdS/CFT) approach [78,79], which effectively accounts for higher quark Fock space configurations, provides a good description of the $N(1440)1/2^+$ and $N(1535)1/2^-$ electrocouplings over the entire Q^2 range, but with the most substantial improvements for low Q^2. This success emphasized the importance in N^* structure of accounting for the meson baryon cloud generated by the higher quark Fock space configurations. The $N(1675)5/2^-$ resonance (see Fig. 10 (bottom left)) in the case of exact SU(6) symmetry and the single-quark transition electromagnetic current should not be excited in the $\gamma_v p$ reaction. SU(6) symmetry breaking results in a small value for the contributions from quarks as evaluated in Refs. [85,86]. These contributions are an order of magnitude smaller than the CLAS electrocoupling results. However, the implementation of the contributions from the meson-baryon cloud [80,81] allows for the description of the $N(1675)5/2^-$ electrocouplings. Therefore, these results for the first time probe the meson-baryon cloud almost completely.

The structure of all N^* states, as revealed by the studies of the electrocouplings, is determined by a complex interplay between the inner core of three dressed quarks and the external meson baryon cloud. The size of the meson-baryon dressing amplitudes is maximal for $Q^2 < 1$ GeV^2. As Q^2 increases there is a transition to the domain where the quark degrees of freedom just begin to dominate, as seen by the improved description of the N^* electrocouplings obtained accounting for the quark core only (see Fig. 10 and Fig. 11) and also Refs. [89, 90]. For $Q^2 > 5$ GeV^2, the quark degrees of freedom are expected to fully dominate the structure of N^* states [91]. Therefore, in the electrocoupling studies for $Q^2 > 5$ GeV^2 that are expected to become available for the first time in the $\pi^+\pi^- p$, πN, ηN, and KY channels with the data from CLAS12 [92,93,94], the quark degrees of freedom will be probed more directly with only minor contributions from the meson-baryon cloud. This will mark the first opportunity to study experimentally this new and unexplored region of quark core dominance
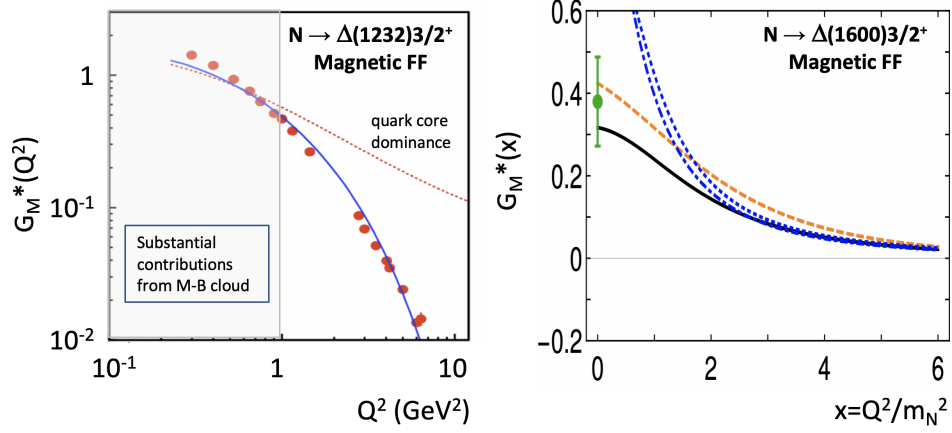
Fig. 12 (Left) Description of the $N \to \Delta(1232)3/2^+$ magnetic transition form factor [37] with frozen (red dashed) and running (solid blue) quark mass [11]. (Right) Prediction for the $N \to \Delta(1600)3/2^+$ magnetic transition form factor within the continuum QCD approach [95,96] with the same momentum dependence of the running mass of the dressed quarks as for the $\Delta(1232)3/2^+$, $N(1440)1/2^+$, and $\Delta(1600)3/2^+$ (black solid line). The DSE evaluations under the assumption that the wave function of the $\Delta(1600)3/2^+$ is reduced to the s-wave component only are shown by the blue lines. The dot-dashed line includes the full wave function of the proton and the dotted line assumes only the s-wave component. The DSE computation with an increased axial vector diquark contribution in the proton wave function is shown by the long-dashed orange line.

in the electroexcitation of nucleon resonances. For the foreseeable future, CLAS12 will be the only facility in the world capable of investigating N^* structure at the distance scale where the dressed quarks emerge from QCD and generate the spectrum of excited nucleon states.

4.2 Emergence of Hadron Mass from CLAS Data and New Opportunities with CLAS12

Studies of the $\gamma_v p N^*$ electrocouplings shed light on the strong QCD dynamics that govern the generation of the dominant part of hadron mass [7,11,14,15]. In resonance electroexcitation, the virtual photon interaction with the dressed quarks is sensitive to the dressed quark propagator. Hence, by varying Q^2, it become possible to map out the momentum dependence of the dressed quark mass through its manifestation in the Q^2-evolution of the electrocouplings.

The first evaluations of the $\Delta(1232)3/2^+$, $N(1440)1/2^+$, and $\Delta(1600)3/2^+$ electrocouplings starting from the QCD Lagrangian have become available from the continuum QCD DSE approach [11,12,13,14,95,96] for $Q^2 < 12\,\mathrm{GeV}^2$. As was discussed in Section 4.1, the resonance structure is defined by a complex interplay between the inner core of three dressed quarks and the external meson-baryon cloud. Currently, the DSE evaluations account for only the quark core component and can be directly confronted to the experimental results on the resonance electrocouplings only at high enough Q^2 where the contributions from the quark core play a major role.

The continuum QCD evaluations of the $N \to \Delta$ magnetic transition form factor and the $A_{1/2}$ electrocoupling of the $N(1440)1/2^+$ are shown in Fig. 9 (left) and Fig. 12 (left). A good description of the experimental results has been achieved at Q^2 where the contributions from the quark core substantially exceed those from the meson-baryon cloud ($Q^2 > 0.8\,\mathrm{GeV}^2$ for the $\Delta(1232)3/2^+$ and $Q^2 > 2\,\mathrm{GeV}^2$ for the $N(1440)1/2^+$). The continuum QCD evaluations of the $N \to \Delta$ magnetic transition form factor [11] shown in Fig. 12 (left) were carried out by using two different ansätze for the qq-interaction. In the initial exploratory computations,

the results were obtained by using a simplified qq contact interaction that accounts for the dynamical generation of the dressed quark mass of ≈ 350 MeV, but predicts the dressed quark mass independent of the quark momentum. The $N \to \Delta$ magnetic form factor computed with this frozen quark mass (shown in Fig. 12 (left) by the dashed red line), overestimates the experimental results for $Q^2 > 1$ GeV^2, with the discrepancy increasing with Q^2. Eventually, this simplified description was replaced by the most advanced ansatz for the qq-interaction [97, 98, 99] that employs a dressed gluon propagator supported by the computations from the gauge sector of QCD [100]. The dressed quark propagator obtained as the solution of the gap equation by employing this advanced ansatz corresponds to a momentum-dependent (running) mass for the dressed quarks as shown in Fig. 1 (right). The continuum QCD evaluation, which incorporates the running mass of the dressed quarks, provides a good description of the experimental results on the Q^2-evolution of the $N \to \Delta$ magnetic transition form factor for $Q^2 > 0.8$ GeV^2 (shown in Fig. 12 by the solid blue line). Analysis of the CLAS results on the $N \to \Delta$ magnetic transition form factor [37] within the continuum QCD approach [11] have conclusively demonstrated that the mass of the dressed quarks is running with the quark momentum.

Remarkably, a successful description of the $N(1440)1/2^+$ electroexcitation amplitudes for $Q^2 > 2$ GeV^2 (see Fig. 9 (left)) has been achieved with the dressed quark mass function evaluated under connection to the QCD Lagrangian that is *the same* as that used previously in the successful description of the pion [101], nucleon elastic, and $N \to \Delta$ transition magnetic form factors [11, 102]. Therefore, the consistent results on the momentum dependence of the running dressed quark mass have become available from the independent studies of the pion and nucleon elastic form factors, as well as from analyses of the electroexcitation amplitudes of nucleon resonances of distinctively different structure, the $\Delta(1232)3/2^+$ (the spin-isospin flip of three dressed quarks) and the $N(1440)1/2^+$ (the first radial excitation of three dressed quarks). This success validates the relevance of dressed quarks with a momentum-dependent mass inferred from the QCD Lagrangian as the dynamical constituents in the structure of the ground state pion, the nucleon, and the lowest excited nucleon states. The capability to map out the momentum dependence of the dressed quark mass from analyses of the results on the Q^2-evolution of the nucleon elastic form factors and the electrocouplings has been conclusively demonstrated. A successful description of these quantities for prominent N^* states with the same dressed quark mass function is critical in order to validate insight into this key ingredient of strong QCD. Insight into the strong QCD dynamics that control the generation of $>98\%$ of the mass of hadrons from the results on the nucleon elastic form factor and the $\gamma_v p N^*$ electrocouplings represents one of the most impressive achievements in hadron physics of the last decade in the synergistic efforts between experiment, phenomenology, and theory.

The continuum QCD approach [95, 96] has provided a parameter-free prediction on the Q^2-evolution of $N \to \Delta(1600)3/2^+$ $G_M^*(Q^2)$ magnetic transition form factor with the dressed quark mass function and all other elements in the Faddeev kernel for evaluation of the resonance mass and wave function exactly the same as used for the successful description of the electroexcitation amplitudes of the $\Delta(1232)3/2^+$ and $N(1440)1/2^+$ (see Fig. 12 (right)). These predictions will be confronted with the experimental results from CLAS on the electroexcitation amplitudes of the $\Delta(1600)3/2^+$ that are expected in the near-term future.

From the measurements with the CLAS12 detector outlined in Section 4.1, the results on the electrocouplings will be extended toward the highest Q^2 ever achieved in exclusive meson electroproduction data of > 5 GeV^2. The expected quality of the results should be comparable to or better than those already available. The data expected from the experiments of the N^* program with CLAS12 will make possible the study of the kinematic regime of quark momenta $0.5 < p < 1.1$ GeV (where $p = \sqrt{Q^2/3}$), running over the dressed-quark propagator (see Fig. 1 (right)). The electrocouplings will be sensitive to the transition from the confinement regime

of strongly bound dressed quarks and gluons at small momenta ($p < 0.5$ GeV) to the pQCD regime ($p > 2$ GeV), where almost undressed and weakly interacting current quarks and gauge gluons gradually emerge as the relevant degrees of freedom in the resonance structure with increasing Q^2. Consistent results on the dressed quark mass function from the independent analyses of the electrocouplings of all prominent nucleon resonances of different structure, including different spin-isospin flips, radial, and orbital three-quark excitations, will validate insight into this key ingredient of strong QCD.

Studies of the N^* electroexcitations with CLAS12 will address key open problems in the Standard Model on the nature of hadron mass, its emergence from QCD, and its connection with DCSB. With the dressed quark mass function checked against the data on the nucleon elastic form factors and the electrocouplings, the continuum QCD approach will be able to compute the parton pressure distributions in the nucleon ground state and to address another key open problem of the Standard Model on the emergence of quark-gluon confinement. A recent breakthrough in the studies of deeply virtual Compton scattering (DVCS) with CLAS [103] has demonstrated the capability to gain insight into the parton pressure distribution. The accuracy of these results is expected to increase dramatically from the data of the DVCS experiments with CLAS12.

5 Conclusions and Outlook

Impressive progress has been achieved in the studies of nucleon resonance structure from the data on exclusive meson electroproduction. Such high-quality data from CLAS have allowed us to determine the electrocouplings of most resonances in the mass range up to 1.8 GeV with consistent results from analyses of the $\pi^+ n$, $\pi^0 p$, ηp, and $\pi^+\pi^- p$ channels [2,3,4]. This good agreement allows us to evaluate the systematic uncertainties for the electrocouplings related to the use of the reaction models. The analyses of the recent CLAS data on πN and $\pi^+\pi^- p$ electroproduction [27,45,46] will further extend the information on the $\gamma_v p N^*$ electrocouplings for most N^* states in the mass range up to 2 GeV for $0.2 < Q^2 < 5$ GeV^2 in the near-term future [20,21]. The combined analyses of photo- and electroproduction data offer a promising new avenue in the exploration of the N^* spectrum as was demonstrated in the recent observation of the new $N'(1720)3/2^+$ state from the $\pi^+\pi^- p$ data [19]. The extension of the coupled-channel approaches successfully used for the search for missing resonances from the photoproduction data [18,104] toward the combined analyses of exclusive photo- and electroproduction data is of particular importance in order to obtain the ultimate information on the spectrum of N^* states generated in the strong QCD regime within the current decade. These developments will also facilitate the search for a new type of hybrid N^* state with glue as an active structural component in experiments with the CLAS12 detector [105,106].

Analyses of the results on the N^* electrocouplings [2,3,15,37] within the continuum QCD approach [11,12,13,14], quark models [16,74,78,79], and the Argonne-Osaka global multichannel framework [17,104] have revealed that the structure of all N^* states studied with CLAS can be understood in terms of a complex interplay between an inner core of three dressed quarks and an external meson-baryon cloud. Future studies of the CLAS12 results on the nucleon resonance electrocouplings in the synergistic efforts between the continuum and lattice QCD approaches, and global coupled-channel analyses extended for the description of exclusive electroproduction, will shed light on the transition from confined dressed quarks in the resonance quark core to the meson-baryon cloud. These joint efforts between experiment and theory will address an important open problem on how quark-gluon confinement transforms into hadronic interactions between mesons and baryons.

The experimental results on the electrocouplings have provided important insights into the strong QCD dynamics that underlie the dominant part of hadron mass generation. The successful description of the CLAS results on the electrocouplings of the $\Delta(1232)3/2^+$ and $N(1440)1/2^+$ [15,20,37,67] within the continuum QCD approach [11,14], achieved with the *same* dressed quark mass function computed from the QCD Lagrangian, have demonstrated the capability to gain insight into this key ingredient of strong QCD. Furthermore, consistent results on the momentum dependence of the dressed quark mass from independent studies of the electrocouplings of nucleon resonances with distinctively different structure is critical in order to validate insight into the dynamics of hadron mass generation in a nearly model-independent way. The continuum QCD approach [95,96] has provided a parameter-free prediction for the electrocouplings of the $\Delta(1600)3/2^+$ by employing a universal quark mass function for the ground and excited nucleon states. The extraction of the resonance electrocouplings from the CLAS $\pi^+\pi^-p$ electroproduction data [45,46] is in progress. Confirmation of the continuum QCD expectations on the electroexcitation amplitudes of this state will validate credible insight into the dynamics of hadron mass generation for $Q^2 < 5$ GeV^2 covered by these data. Extension of the results on the electrocouplings toward $Q^2 > 5$ GeV^2 expected from the N^* program with CLAS12 will allow us to map out the momentum dependence of the dressed quark mass at distances where the transition from quark-gluon confinement to pQCD is expected. These results will address a key open problem of the Standard Model on the emergence of hadron mass from QCD.

Theoretically, continuum QCD approaches, which employ a well-constrained dressed quark mass function and diquark correlation amplitudes mapped out in studies of the experimental results on the nucleon elastic form factors and the electrocouplings, are capable of evaluating the light-front wave function of the nucleon. This quantity can yield a complete theoretical description of the nucleon's shape in its intrinsic frame. Moreover, addressing the emergence of the dynamical deformation seen in the structure of atomic nuclei, the continuum QCD approach can also describe the pion-exchange part of the NN-interaction with a πNN vertex inferred from strong QCD within the same framework used for the description of the nucleon shape. Synergistic efforts in the experimental studies of the ground state nucleon and N^* structure, combined with the developments in continuum QCD approaches and the theory of atomic nuclear structure [107,108], pave the way toward understanding how the structure of atomic nuclei emerges from strong QCD [4].

The dressed quark mass function that unifies the experimental results on the nucleon elastic form factors and the electrocouplings can also be used for the computation of the pion electromagnetic form factors and parton distribution functions (PDFs) within continuum QCD approaches. Hence, any conclusions drawn about the dynamics of hadron mass generation through studies of ground/excited-state nucleon structure can be validated via comparisons between the experimental results on the pion form factors/PDFs and the predictions from continuum QCD obtained with the same dressed quark mass function [4,10,101].

The experiments in the 12 GeV era at Jefferson Lab with the CLAS12 detector, in conjunction with the completed and planned measurements with the datasets from the CLAS, offer a unique opportunity to map out the momentum dependence of the quark running mass at distances that correspond to the transition from bare QCD quarks to fully dressed constituent quarks. Insight into the dressed quark running mass from the experimental results on meson and baryon structure within the common framework offered by the continuum QCD approach will elucidate the emergence of $>98\%$ of the hadron mass in the universe and how the structure of atomic nuclei is generated in the strong QCD regime. These objectives can be achieved in synergistic efforts between experiment, phenomenology, and the theory of hadron/nuclear structure with a traceable connection to QCD.

References

1. V.D. Burkert and C.D. Roberts, *Roper Resonance: Toward a Solution to the Fifty Year Puzzle*, Rev. Mod. Phys. **91**, 011003 (2019).
2. I.G. Aznauryan and V.D. Burkert, *Electroexcitation of Nucleon Resonances*, Prog. Part. Nucl. Phys. **67**, 1 (2012).
3. V.I. Mokeev *(CLAS Collaboration)*, *Nucleon Resonance Structure from Exclusive Meson Electroproduction with CLAS*, Few Body Syst. **59**, 46 (2018).
4. S.J. Brodsky *et al.*, *QCD2019 Workshop*, arXiv:2006.06802 [hep-ph].
5. C. Mezrag *et al.*, *Parton Distribution Amplitudes: Revealing Correlations Within the Proton and Roper*, Phys. Lett. B **783**, 263 (2018).
6. A.N. Hiller Blin *et al.*, *Nucleon Resonance Contributions to Unpolarized Inclusive Electron Scattering*, Phys. Rev. C **100**, 035201 (2019).
7. C.D. Roberts, *N^* Structure and Strong QCD*, Few Body Syst. **59**, 72 (2018).
8. C.D. Roberts, *Three Lectures on Hadron Physics*, J. Phys. Conf. Ser. **706**, 022002 (2016).
9. Chen Chen *et al.*, *Structure of the Nucleons Low-Lying Excitations*, Phys. Rev. D **97**, 034016 (2018).
10. A.C. Aguilar *et al.*, *Pion and Kaon Structure at the Electron-Ion Collider*, Eur. Phys. J. A **55**, 190 (2019).
11. J. Segovia, I.C. Cloet, C.D. Roberts, and S.M. Schmidt, *Elastic and Transition Form Factors of the $\Delta(1232)$*, Few Body Syst. **55**, 1185 (2014).
12. J. Segovia and C.D. Roberts, *Dissecting Nucleon Transition Electromagnetic Form Factors*, Phys. Rev. C **94**, 042201 (2016).
13. Chen Chen *et al.*, *Nucleon-to-Roper Electromagnetic Transition Form Factors at Large Q^2*, Phys. Rev. D **99**, 034013 (2019).
14. J. Segovia, B. El-Bennich, E. Rojas, I. C. Cloet, C.D. Roberts, S.-S. Xu, and H.-S. Zong, *Completing the Picture of the Roper Resonance*, Phys. Rev. Lett. **115**, 171801 (2015).
15. V.I. Mokeev *et al.*, *New Results from the Studies of the $N(1440)1/2^+$, $N(1520)3/2^-$, and $\Delta(1620)1/2^-$ Resonances in Exclusive $ep \to e'p'\pi^+\pi^-$ Electroproduction with the CLAS Detector*, Phys. Rev. C **93**, 025206 (2016).
16. I.T. Obukhovsky *et al.*, *Transition Form Factors and Helicity Amplitudes for Electroexcitation of Negative and Positive Parity Nucleon Resonances in a Light-Front Quark Model*, Phys. Rev. D **100**, 094013 (2019).
17. H. Kamano, *Electromagnetic N^* Transition Form Factors in the ANL-Osaka Dynamical Coupled-Channels Approach*, Few Body Syst. **59**, 24 (2018).
18. A.V. Anisovich *et al.*, *Strong Evidence for Nucleon Resonances Near 1900 MeV*, Phys. Rev. Lett. **119**, 062004 (2017).
19. V.I. Mokeev *et al.*, *Evidence for the $N'(1720)3/2^+$ Nucleon Resonance from Combined Studies of CLAS $\pi^+\pi^-p$ Photo- and Electroproduction Data*, Phys. Lett. B **805**, 135457 (2020).
20. V.I. Mokeev, *Two Pion Photo- and Electroproduction with CLAS*, arXiv:1909.08746 [nucl-ex].
21. V.D. Burkert *et al.*, *The Nucleon Resonance Structure from the $\pi^+\pi^-p$ Electroproduction Reaction off Protons*, Moscow Univ. Phys. Bull. **74**, 243 (2019).
22. V.D. Burkert, *N^* Experiments and Their Impact on Strong QCD Physics*, Few Body Syst. **59**, 57 (2018).
23. B.A. Mecking *et al.*, *The CEBAF Large Acceptance Spectrometer*, Nucl. Inst. and Meth. A **503**, 513 (2003).
24. CLAS Physics Database, http://clasweb.jlab.org/physicsdb
25. V.D. Burkert *et al. (CLAS Collaboration)*, *The CLAS12 Spectrometer at Jefferson Laboratory*, Nucl. Inst. and Meth. A **959**, 163419 (2020).
26. K. Park *et al. (CLAS Collaboration)*, *Measurements of $ep \to e'\pi^+n$ at $W = 1.6$ - 2.0 GeV and Extraction of Nucleon Resonance Electrocouplings at CLAS*, Phys. Rev. C **91**, 045203 (2015).
27. N. Markov *et al. (CLAS Collaboration)*, *Exclusive π^0p Electroproduction off Protons in the Resonance Region at Photon Virtualities 0.4 $GeV^2 \leq Q^2 \leq 1.0$ GeV^2*, Phys. Rev. C **101**, 015208 (2020).
28. K. Joo *et al. (CLAS Collaboration)*, *Q^2 Dependence of Quadrupole Strength in the $\gamma^*p \to \Delta^+(1232) \to p\pi^0$ Transition*, Phys. Rev. Lett. **88**, 122001 (2002).

29. H. Egiyan *et al. (CLAS Collaboration)*, *Single π^+ Electroproduction on the Proton in the First and Second Resonance Regions at 0.25 $GeV^2 < Q^2 < 0.65$ GeV^2 using CLAS*, Phys. Rev. C **73**, 025204 (2006).
30. K. Park *et al. (CLAS Collaboration)*, *Cross Sections and Beam Asymmetries for $ep \to en\pi^+$ in the Nucleon Resonance Region for $1.7 < Q^2 < 4.5$ GeV^2*, Phys. Rev. C **77**, 015208 (2008).
31. M. Ungaro *et al. (CLAS Collaboration)*, *Measurement of $N \to \Delta(1232)$ Transition at High Momentum Transfer by π^0 Electroproduction*, Phys. Rev. Lett. **97**, 112003 (2006).
32. K. Joo *et al. (CLAS Collaboration)*, *Measurement of the Polarized Structure Function $\sigma_{LT'}$ for Pion Electroproduction in the Roper Resonance Region*, Phys. Rev. C **72**, 058202 (2005).
33. K. Joo *et al. (CLAS Collaboration)*, *Measurement of the Polarized Structure Function $\sigma_{LT'}$ for $p(e, e'\pi^+)n$ in the $\Delta(1232)$ Resonance Region*, Phys. Rev. C **70**, 042201 (2004).
34. K. Joo *et al. (CLAS Collaboration)*, *Measurement of the Polarized Structure unction $\sigma_{LT'}$ for $p(e, e'\pi^0)n$ in the $\Delta(1232)$ Resonance Region*, Phys. Rev. C **68**, 032201 (2003).
35. A. Biselli *et al. (CLAS Collaboration)*, *Study of $ep \to ep\pi^0$ in the $\Delta(1232)$ Mass Region Using Polarization Asymmetries*, Phys. Rev. C **68**, 035202 (2003).
36. I.G. Aznauryan, *Multipole Amplitudes of Pion Photoproduction on Nucleons up to 2 GeV Within Dispersion Relations and Unitary Isobar Model*, Phys. Rev. C **67**, 015209 (2003).
37. I. Aznauryan *et al. (CLAS Collaboration)*, *Electroexcitation of Nucleon Resonances from CLAS Data on Single Pion Electroproduction*, Phys. Rev. C **80**, 055203 (2009).
38. M. Tanabashi *et al. (Particle Data Group)*, *Review of Particle Physics*, Phys. Rev. D **98**, 03001 (2018).
39. S. Capstick and W. Roberts, *Quasi Two-body Decays of Non-Strange Baryons*, Phys. Rev. D **49**, 4570 (1994).
40. R. Bijker *et al.*, *Strong Decays of Baryons and Missing Resonances*, Phys. Rev. D **94**, 074040 (2016).
41. E. Golovatch *et al. (CLAS Collaboration)*, *First Results on Nucleon Resonance Photocouplings from the $\gamma p \to \pi^+\pi^- p$ Reaction*, Phys. Lett. B **788**, 371 (2019).
42. G.V. Fedotov *et al.*, *(CLAS Collaboration)*, *Electroproduction of $p\pi^+\pi^-$ off Protons at $0.2 < Q^2 < 0.6$ GeV^2 and $1.3 < W < 1.57$ GeV with CLAS*, Phys. Rev. C **79**, 015204 (2009).
43. M. Ripani *et al. (CLAS Collaboration)*, *Measurement of $ep \to e'p\pi^+\pi^-$ and Baryon Resonance Analysis*, Phys. Rev. Lett. **91**, 022002 (2003).
44. G.V. Fedotov *et al. (CLAS Collaboration)*, *Measurements of the $\gamma_v p \to p'\pi^+\pi^-$ Cross Section with the CLAS Detector for 0.4 $GeV^2 < Q^2 < 1.0$ GeV^2 and 1.3 $GeV < W < 1.825$ GeV*, Phys. Rev. C **98**, 025203 (2018).
45. E.L. Isupov *et al. (CLAS Collaboration)*, *Measurements of $ep \to e'\pi^+\pi^-$ Cross Sections with CLAS at 1.40 $GeV < W < 2.0$ GeV and 2.0 $GeV^2 < Q^2 < 5.0$ GeV^2*, Phys. Rev. C **96**, 025209 (2017).
46. A. Trivedi, *Measurement of New Observables from the $\pi^+\pi^- p$ Electroproduction Off the Proton*, Few Body Syst. **60**, 1 (2019).
47. R.K. Bradford *et al. (CLAS Collaboration)*, *Differential Cross Sections for $\gamma + p \to K^+ + Y$ for Λ and Σ^0 Hyperons*, Phys. Rev. C **73**, 035202 (2006).
48. R.K. Bradford *et al. (CLAS Collaboration)*, *First Measurement of Beam-Recoil Observables $C(x)$ and $C(z)$ in Hyperon Photoproduction*, Phys. Rev. C **75**, 035205 (2007).
49. M.E. McCracken *et al. (CLAS Collaboration)*, *Differential Cross Section and Recoil Polarization Measurements for the $\gamma p \to K^+\Lambda$ Reaction Using CLAS at Jefferson Lab*, Phys. Rev. C **81**, 025201 (2010).
50. B. Dey *et al. (CLAS Collaboration)*, *Differential Cross Sections and Recoil Polarizations for the Reaction $\gamma p \to K^+\Sigma^0$*, Phys. Rev. C **82**, 025202 (2010).
51. D.S. Carman, *Nucleon Structure Studies via Exclusive KY Electroproduction*, Few Body Syst. **57**, 941 (2016).
52. D.S. Carman, *CLAS N* Excitation Results from Pion and Kaon Electroproduction*, Few Body Syst. **59**, 82 (2018).
53. B.A. Raue and D.S. Carman, *Ratio of σ_L/σ_T for $p(e, e'K^+)\Lambda$ Extracted from Polarization Transfer*, Phys. Rev. C **71**, 065209 (2005).
54. P. Ambrozewicz *et al. (CLAS Collaboration)*, *Separated Structure Functions for the Exclusive Electroproduction of $K^+\Lambda$ and $K^+\Sigma^0$ Final States*, Phys. Rev. C **75**, 045203 (2007).
55. R. Nasseripour *et al. (CLAS Collaboration)*, *Polarized Structure Function $\sigma_{LT'}$ for $p(e, e'K^+)\Lambda$ in the Nucleon Resonance Region*, Phys. Rev. C **77**, 065208 (2008).
56. D.S. Carman *et al. (CLAS Collaboration)*, *Separated Structure Functions for Exclusive $K^+\Lambda$ and $K^+\Sigma^0$ Electroproduction at 5.5 GeV at CLAS*, Phys. Rev. C **87**, 025204 (2013).
57. M. Gabrielyan *et al. (CLAS Collaboration)*, *Induced Polarization of $\Lambda(1116)$ in Kaon Electroproduction*, Phys. Rev. C **90**, 035202 (2014).
58. D.S. Carman *et al. (CLAS Collaboration)*, *First Measurement of Transferred Polarization in the Exclusive $ep \to e'K^+\Lambda$ Reaction*, Phys. Rev. Lett. **90**, 131804 (2003).

59. D.S. Carman *et al. (CLAS Collaboration)*, *Beam-Recoil Polarization Transfer in the Nucleon Resonance Region in the Exclusive $ep \to e'K^+\Lambda$ and $ep \to e'K^+\Sigma^0$ Reactions*, Phys. Rev. C **79**, 065205 (2009).

60. T. Corthals *et al.*, *Electroproduction of Kaons from the Proton in a Regge-plus-resonance Approach*, Phys. Lett. B **656**, 186 (2007).

61. D. Rönchen *et al.*, *The Impact of $K^+\Lambda$ Photoproduction on the Resonance Spectrum*, Eur. Phys. J. A **54**, 110 (2018).

62. L. Tiator, *The MAID Legacy and Future*, Few Body Syst. **59**, 21 (2018).

63. L. Tiator, *Electromagnetic Excitation of Nucleon Resonances*, Eur. Phys. J. ST **198**, 141 (2011).

64. R.A. Arndt *et al.*, *Baryon Resonance Analysis from SAID*, Chin. Phys. C **33**, 1063 (2009).

65. H. Denizli, *Q^2 Dependence of the $S_{11}(1535)$ Photocoupling and Evidence for a P-wave Resonance in η Electroproduction*, Phys. Rev. C **76**, 015204 (2007).

66. V.I. Mokeev *et al.*, *Model Analysis of the $p\pi^+\pi^-$ Electroproduction Reaction on the Proton*, Phys. Rev. C **80**, 045212 (2009).

67. V.I. Mokeev *et al. (CLAS Collaboration)*, *Experimental Study of the $P_{11}(1440)$ and $D_{13}(1520)$ resonances from CLAS data on $ep \to e'\pi^+\pi^-p'$*, Phys. Rev. C **86**, 035203 (2012).

68. V.D. Burkert *et al.*, *Isobar Channels in the Production of $\pi^+\pi^-$ Pairs on a Proton by Virtual Photons*, Phys. Atom. Nucl **70**, 427 (2007).

69. M. Ripani *et al.*, *A Phenomenological Description of $\pi^-\Delta^{++}$ Photoproduction and Electroproduction in Nucleon Resonance Region*, Nucl. Phys. A **672**, 220 (2000).

70. A. Villano *et al.*, *Neutral Pion Electroproduction in the Resonance Region at High Q^2*, Phys. Rev. C **80**, 035203 (2009).

71. M.M. Dalton *et al.*, *Electroproduction of Eta Mesons in the $S(11)(1535)$ Resonance Region at High Momentum Transfer*, Phys. Rev. C **80**, 015205 (2009).

72. J. Rodriguez-Quintero *et al.*, *Form factors for the Nucleon-to-Roper Electromagnetic Transition at Large Q^2*, arXiv:1909.13793 [nucl-th].

73. C.D. Roberts, *Resonance Electroproduction and the Origin of Mass*, arXiv;1909.11102 [nucl-th].

74. I.G. Aznauryan and V.D. Burkert, *Electroexcitation of Nucleon Resonances in a Light-Front Relativistic Quark Model*, Few. Body Syst. **59** 5, 98 (2018).

75. N. Isgur and G. Karl, *Positive Parity Excited Baryons in a Quark Model with Hyperfine Interactions*, Phys. Rev. D **19**, 2653 (1979).

76. S. Capstick and N. Isgur, *Baryons in a Relativized Quark Model with Chromodynamics*, Phys. Rev. D **34**, 2809 (1986).

77. M.M. Giannini and E. Santopinto, *The Hypercentral Constituent Quark Model and its Application to Baryon Properties*, Chin. J. Phys. **53**, 020301 (2015).

78. T. Gutsche *et al.*, *Electromagnetic Structure of Nucleon and Roper in Soft-wall AdS/QCD*, Phys. Rev. D **97**, 054011 (2018).

79. T. Gutsche *et al.*, *$\gamma N \to N^*(1535)$ Transition in Soft-wall AdS/QCD*, Phys. Rev. D **101**, 034026 (2020).

80. N. Suzuki *et al.*, *Extraction of Electromagnetic Transition Form Factors for Nucleon Resonances within a Dynamical Coupled-Channels Model*, Phys. Rev. C **82**, 045206 (2010).

81. T. Sato and T-S. H. Lee, *Dynamical Study of the Delta Excitation in $N(e,e'\pi)$ Reactions*, Phys. Rev. C **63**, 055201 (2001).

82. V. Pascalutsa *et al.*, *Electromagnetic Excitation of the $\Delta(1232)$-Resonance*, Phys. Rept. **437**, 125 (2007).

83. I.G. Aznauryan and V.D. Burkert, *Nucleon Electromagnetic Form Factors and Electroexcitation of Low Lying Nucleon Resonances in a Light-Front Relativistic Quark Model*, Phys. Rev. C **85**, 055202 (2012).

84. I.G. Aznauryan and V.D. Burkert, *Extracting Meson-Baryon Contributions to the Electroexcitation of the $N(1675)5/2^-$ Nucleon Resonance*, Phys. Rev. C **92**, 015203 (2015).

85. E. Santopinto and M.M. Giannini, *Systematic Study of Longitudinal and Transverse Helicity Amplitudes in the Hypercentral Constituent Quark Model*, Phys. Rev. C **86**, 065202 (2012).

86. D. Merten *et al,*, *Electromagnetic Properties of Baryons in a Relativistic Quark Model*, Eur. Phys. J. A **18**, 125 (2003).

87. B. Julia-Diaz *et al.*, *Dynamical Coupled-Channels Effects on Pion Photoproduction*, Phys. Rev. C **77**, 045205 (2012).

88. M.Sun *et al.*, *Roper State from Overlap Fermions*, Phys. Rev. D **101**, 054511 (2020).

89. G. Ramalho and M.T. Pena, *$\gamma^*N \to N^*(1520)$ Form Factors in the Space-like Region*, Phys. Rev. D **89**, 094016 (2014).

90. G. Ramalho, *Using the Single Quark Transition Model to Predict Nucleon Resonance Amplitudes*, Phys. Rev. D **90**, 033010 (2014).

91. I.G. Aznauryan *et al.*, *Studies of Nucleon Resonance Structure in Exclusive Meson Electroproduction*, Int. J. Mod. Phys. **E22**, 1330015 (2013).

92. JLab CLAS12 Experiment E12-09-003, *Nucleon Resonance Studies with CLAS12*, Spokespersons: R.W. Gothe, V.D. Burkert, P. Cole, K. Joo, V.I. Mokeev, P. Stoler.

93. JLab CLAS12 Experiment E12-06-108A, *Exclusive $N^* \to KY$ Studies with CLAS12*, Spokespersons: D.S. Carman, R.W. Gothe, V.I. Mokeev.

94. JLab CLAS12 Experiment E12-16-010a, *Nucleon Resonance Structure Studies Via Exclusive KY Electroproduction at 6.6 GeV and 8.8 GeV*, Spokespersons: D.S. Carman, R.W. Gothe, V.I. Mokeev.

95. J. Segovia *et al.*, *Nucleon-to-Resonance Form Factors at Large Photon Virtualities*, arXiv:1908.05729 [nucl-th].

96. Ya Lu *et al.*, *Transition Form Factors: $\gamma^* + p \to \Delta(1232), \Delta(1600)$*, Phys. Rev. D **100**, 034001 (2019).

97. L. Chang *et al.*, *Dressed-Quark Anomalous Magnetic Moments*, Phys. Rev. Lett. **106**, 072001 (2011).

98. L. Chang *et al.*, *Imaging Dynamical Chiral Symmetry Breaking: Pion Wave Function on the Light Front*, Phys. Rev. Lett. **110**, 132001 (2013).

99. L. Chang *et al.*, *Light Front Distribution of the Chiral Condensate*, Phys. Lett. B **727**, 255 (2013).

100. D. Binosi *et al.*, *Bridging a Gap Between Continuum-QCD and ab initio Predictions of Hadron Observables*, Phys. Lett. B **742**, 183 (2015).

101. T. Horn and C.D. Roberts, *The Pion: an Enigma Within the Standard Model*, J. Phys. G **43**, 073001 (2016).

102. Zhu-Fang Cui *et al.*, *Nucleon Elastic Form Factors at Accessible Large Space-like Momenta*, arXiv:2006.11655 [hep-ph].

103. V.D. Burkert, L. Elouadrhiri, and F.-X. Girod, *The Pressure Distribution Inside the Proton*, Nature **557**, 7705, 396 (2018).

104. H. Kamano *et al.*, *The ANL-Osaka Partial-Wave Amplitudes of πN and γN Reactions*, arXiv:1909.11935 [nucl-th], (2019).

105. V.D. Burkert, *N^* Experiments and What They Tell us About Strong QCD Physics*, arXiv:1912.11400 [nucl-ex], (2019).

106. JLab CLAS12 Experiment E12-16-010, *A Search for Hybrid Baryons in Hall B with CLAS12*, Spokespersons: A. D'Angelo, V.D. Burkert, D.S Carman, E. Golovatch, R.W. Gothe, V.I Mokeev.

107. K.D. Launey *et al.*, *Symmetry-Guided Large-Scale Shell-Model Theory*, Prog. Part. Nucl. Phys. **89**, 101 (2016).

108. T. Dytrych *et al.*, *Physics of Nuclei: Key Role of an Emergent Symmetry*, Phys. Rev. Lett. **124**, 042501 (2020).